Multimode transitions of the tetrahedral MO_4 units (M=Si,Ge,Ti) in sillenite single crystals

R. Capelletti and P. Beneventi
Istituto Nazionale per la Fisica della Materia (INFM), Physics Department, University of Parma, Parco Area delle Scienze 7/A, 43100 Parma, Italy

L. Kovács
Crystal Physics Laboratory, Research Institute for Solid State Physics and Optics, Hungarian Academy of Sciences, H-1112 Budapest, Konkoly-Thege út 29-33, Hungary

W. B. Fowler
Department of Physics and Sherman Fairchild Laboratory, Lehigh University, Bethlehem, Pennsylvania 18015
(Received 7 June 2002; published 27 November 2002)

Multimode transitions of the tetrahedral unit modes in $Bi_{12}SiO_{20}$ (BSO), $Bi_{12}GeO_{20}$ (BGO), $Bi_{12}TiO_{20}$ (BTO), and mixed $(1-x)$BSO·xBGO sillenite crystals have been studied using Fourier transform infrared absorption spectroscopy, with a resolution as fine as 0.04 cm^{-1} in the 600–3500-cm^{-1} wave number and 9–300-K temperature ranges. Up to four-mode transitions (overtones of the F mode and combinations of F and A modes) were detected in BGO, BSO, and BTO, and up to three-mode transitions in the mixed crystals. The F-mode anharmonicity parameter, evaluated in the framework of the Morse oscillator model, was in the range 0.003–0.006. The A-mode anharmonicity was found to be still lower. Fine structures of the F-mode absorption were observed and attributed to the LO-TO splitting of the F mode; in the case of BSO, additional structures due to the natural abundance of Si isotopes were detected. The transitions monitored in the mixed crystals were well described by a two-mode behavior. The temperature dependence of the line position and width was studied as well. ''Red'' and ''blue'' shifts were observed for different lines: the results were analyzed by considering thermal expansion and anharmonicity effects.

DOI: 10.1103/PhysRevB.66.174307 PACS number(s): 78.30.Am, 63.20.Pw, 63.20.Ry

I. INTRODUCTION

$Bi_{12}SiO_{20}$ (BSO), $Bi_{12}GeO_{20}$ (BGO) and $Bi_{12}TiO_{20}$ (BTO) sillenite single crystals are large gap semiconductors. They exhibit many interesting properties such as photoconductivity, the electro-optic effect, piezoelectricity, and photorefractivity. Such properties make these materials attractive for technological applications in the fields of optical memories, holography, and optical phase conjugating devices.[1–3] Many important properties of sillenites exploited for different applications are either determined or affected by impurities. Many dopants, present even in small concentrations, can be monitored by means of absorption spectroscopy. Therefore, it is of key importance to have a complete and detailed knowledge of the absorptions of the host material, in order to separate the intrinsic contributions, even the weak ones as, for example, those due to multiphonon transitions, from the extrinsic ones, coming from electronic and vibrational transitions induced by impurities.

Sillenite single crystals have a bcc structure with the MO_4 tetrahedra (M=Si,Ge,Ti) located at the corners and at the center of the cubic unit cell.[4] An interesting feature of these crystals is the presence of only one non-bismuth metal atom in a formula unit of 33 atoms. Thus, for example, in BSO there is only one Si for every 12 Bi, and only four of 20 oxygens are involved in SiO_4 tetrahedra.

Furthermore, Bi is so massive that to a first approximation it defines a fixed matrix surrounding each SiO_4 tetrahedron. This suggests[5] that the part of the phonon spectrum associated with the internal vibrations of MO_4 may be treated as a set of noninteracting (Einstein) oscillators in the sense that the internal vibrations of one SiO_4 tetrahedron will be only weakly coupled to the internal vibrations of other SiO_4 tetrahedra.

The vibrational spectra of sillenites have already been studied by means of infrared (IR) reflectivity,[6,7] absorption,[8] Raman[9–13] spectroscopy measurements, and theoretical calculations.[5] In the wave number region $\omega<600$ cm^{-1} the vibrational frequencies differ only slightly in the different matrices and are attributed to the vibrational modes of Bi and O in Bi_3O_4 and Bi_3O units. For 600 $cm^{-1}<\omega<850$ cm^{-1} the reflectivity and Raman peaks are characteristic of a given matrix and have been attributed to the asymmetric F and symmetric A stretching modes in the MO_4 tetrahedral unit,[5,6,8–13] in agreement with the above assumption that the tetrahedra are weakly coupled to each other. Two- and three-mode transitions related to the tetrahedral unit vibrations have been detected by optical absorption measurements performed mainly at room temperature.[14–17]

In the present work, FTIR absorption spectroscopy in the 600–3500-cm^{-1} wave number and 9–300-K temperature ranges was applied to study the overtone and combination transitions of the tetrahedral unit vibrations (up to four modes) in BSO, BGO, and BTO crystals, and the anharmonicity contributions were evaluated. The analysis was extended to mixed $Bi_{12}Ge_xSi_{1-x}O_{20}$ $[(1-x)$BSO·xBGO$]$ systems to investigate if the two-mode behavior[17,18] could provide a satisfactory description even for the two- and three-mode optical transitions. The use of low temperature and the availability of a resolution as fine as 0.04 cm^{-1} were

TABLE I. Comparison between the nominal Ge fraction (added as BGO to the melt) x and that measured by chemical analysis x_m in $(1-x)$BSO$\cdot x$BGO mixed crystal samples. The chemically determined Si fraction $(1-x)_m$ and the measured (Ref. 19) lattice constant a are also listed.

x (mol/mol)	x_m (mol/mol)	$(1-x)_m$ (mol/mol)	a (Å)
0.25	0.63	0.40	10.121 88±0.004 62
0.5	0.477	0.505	10.108 40±0.012 02
0.75	0.75	0.224	10.124 83±0.011 10

of key importance in detecting fine structures which could otherwise have been missed. Only in this way could a complete description and a unified interpretation of the internal vibration modes of the MO_4 tetrahedral units in the three most important sillenite crystals and in one of their alloys be made possible. Furthermore, a thorough analysis of even fine details, for example the quantitative description of the isotopic and anharmonicity effects, shows how the MO_4 units in materials of technological interest can be regarded as a model system to test basic concepts of vibrational spectroscopy.

II. EXPERIMENTAL DETAILS

The reagent powders used to grow crystals were Bi_2O_3 and GeO_2 prepared from 5N pure metal rods by chemical digestion, while SiO_2 and TiO_2 were Johnson Matthey grade $A1$ oxides.

BSO, BGO, and mixed $(1-x)$BSO$\cdot x$BGO crystals were grown in air by the balance controlled Czochralski technique using resistance heating and platinum crucible.[19] The boules were pulled along the [001] direction. BGO seeds were used for growing mixed crystals. The incongruently melting BTO crystals were grown from solution by the top seeding technique. The melt was prepared from the mixture of Bi_2O_3 and TiO_2 compounds in the molar ratio of 8:1. The crystals were pulled on BGO seeds, along the [001] direction.

In the mixed crystals $(1-x)$BSO$\cdot x$BGO the nominal x fraction was 0.25, 0.5, and 0.75. However, lattice constant measurements[19] and chemical analysis showed that the actual Ge and Si fractions in the crystals were different from the nominal ones, as shown in Table I. The chemical analysis of Si and Ge was performed by means of inductively coupled plasma (ICP) emission spectroscopy.

Weak traces of S were detected in a few samples, as monitored by the characteristic SO_4 vibrational absorptions [Figs. 2(c) and 4(a)]. Oriented samples were cut in the shape of parallelepipeds and the (100) faces were polished. The cross section was ~ 1 cm^2 and the thickness was in the range 0.1–24 mm. To measure the IR spectra in the high absorption region, chips of sillenite single crystals were finely ground and mixed with KBr powders in the weight ratio of 0.01–0.08 g. Pellets were then prepared from the mixed powders, such that the sillenite equivalent thickness in the pellets was only ~ 2 μm.

The optical absorption measurements were performed by means of a Bomem DA8 Fourier transform infrared (FTIR) spectrophotometer operating in the range 200–4000 cm^{-1}, with an apodized resolution as fine as 0.04 cm^{-1}, and equipped with a mercury cadmium telluride detector, cooled at liquid nitrogen temperature. The spectra were recorded in the range 9–300 K, by placing the sample in a 21SC model Cryodine Cryocooler of CTI-Cryogenics.

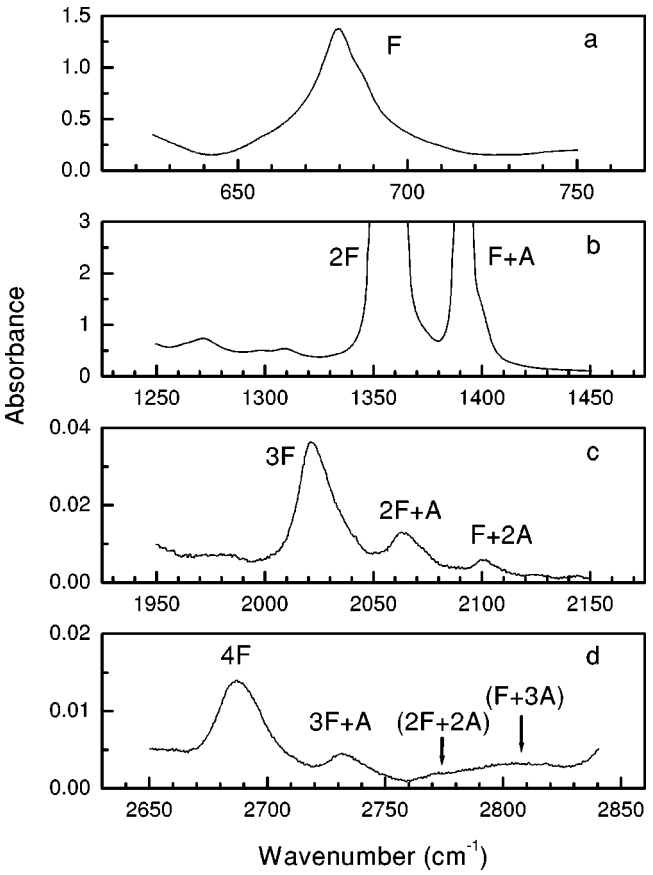

FIG. 1. Optical absorption spectra of BGO single crystals measured at 9 K in different spectral regions: the absorbance is plotted vs the wave number. The spectrum (a) in the low wave number range was measured on a KBr+BGO pellet, due to the high absorption coefficient of BGO. The spectra in the other regions were measured on massive samples of different thicknesses z: $z=1.2$ mm (b), $z=1.2$ mm (c), and $z=40$ mm (d). The assignment of most of the lines to overtones of the F mode and to combinations of F and A modes is shown.

III. RESULTS

BSO, BGO, and BTO samples were analyzed at 9 K by FTIR spectroscopy in the range 600–3500 cm^{-1}. As shown in Fig. 1(a) for BGO, Fig. 2(a) for BTO, and Fig. 3(a) for BSO, a broad, structured peak appears in the spectral range 600–850 cm^{-1}. The absorption spectrum in this region could be measured only on a pellet in which the sillenite equivalent thickness was drastically reduced by the dilution into KBr powders, as noted in Sec. II. In fact, if crystal slices even as thin as 0.1 mm were used, the peak absorbance was out of scale; in this case neither the shape nor the band po-

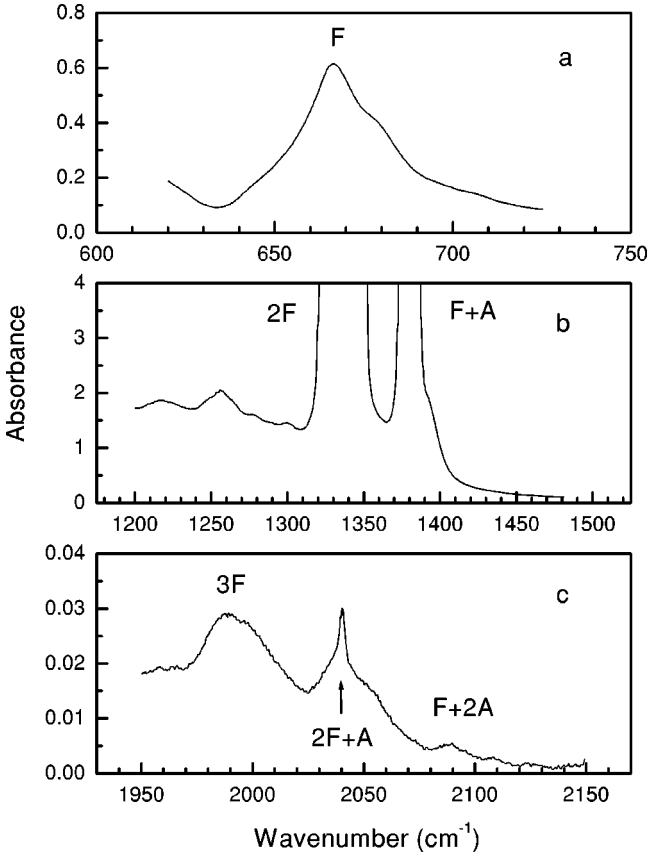

FIG. 2. Optical absorption spectra of BTO single crystals measured at 9 K in different spectral regions: the absorbance is plotted vs the wave number. The spectrum (a) in the short wave number range was measured on a KBr+BTO pellet, due to the high absorption coefficient of BTO. The spectra in the other regions [(b) and (c)] were measured on massive samples of thickness $z=1.2$ mm. The assignment of the most of the lines to overtones of the F mode and to combinations of F and A modes is shown. The narrow line at ~ 2040 cm^{-1}, which overlaps the broader $2F+A$ peak, monitors the presence of S^{6+} traces in the sample, because it originates from an $F+A$ mode excitation of SO_4 tetrahedra (Ref. 21).

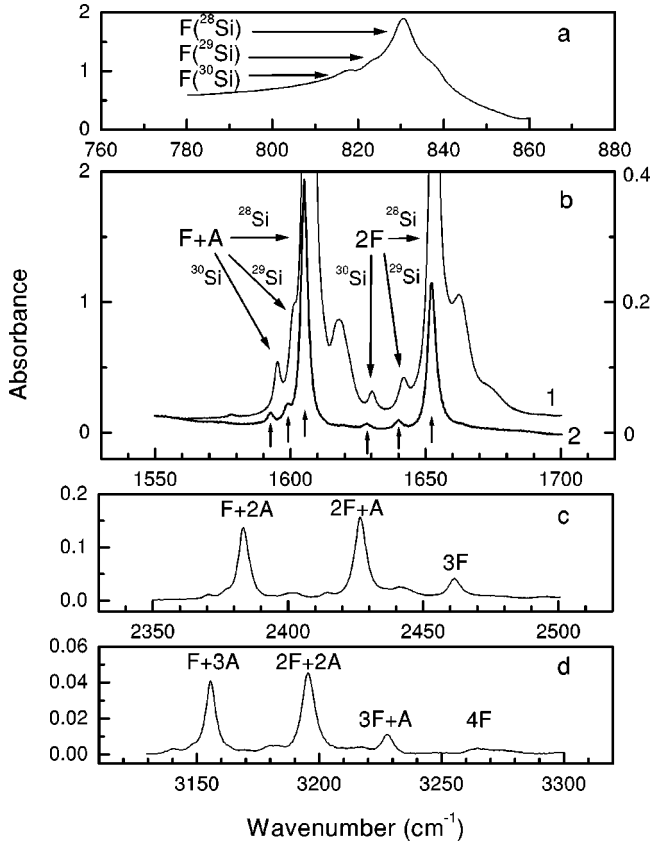

FIG. 3. Optical absorption spectra of BSO single crystals measured at 9 K in different spectral regions: the absorbance is plotted vs the wave number. The spectrum (a) in the low wave number range was measured on a KBr+BSO pellet, due to the high absorption coefficient of BSO. The spectra in the other regions were measured on massive samples of different thicknesses z: $z=1.2$ mm [(b), curve 1], $z=1.2$ mm (c), and $z=24$ mm (d). The assignment of most of the lines to overtones of the F mode and to combinations of F and A modes is shown. In (b), curve 2 is related to a BGO crystal (1.8-mm thick) in which Si is present as an impurity, the atomic fraction Si/Ge being $\sim 3.5\%$. Lines related to different Si isotopes, ^{28}Si, ^{29}Si, and ^{30}Si, respectively, are indicated by arrows.

sition could be accurately determined. Two strong lines were detected in the range 1300–1700 cm^{-1} by measuring the spectra of 1.2-mm-thick samples, as shown in Figs. 1(b) and 2(b) for BGO and BTO, respectively. The BSO spectrum in the same region shows additional weaker bands, as displayed by curve 1 in Fig. 3(b). In the same samples three lines were monitored in the range 2000–2400 cm^{-1}, but they are much weaker; this can be seen by comparing the absorbance scales of Figs. 1(b) and 1(c) for BGO, of Figs. 2(b) and 2(c) for BTO, and of Figs. 3(b) (curve 1) and 3(c) for BSO, respectively. In order to detect the spectra in the range 2600–3300 cm^{-1}, a sandwich of three samples (the total thickness being 40 mm) was used. Four bands were detected in BGO [Fig. 1(d)] and BSO (Ref. 17) [Fig. 3(d)], while only a weak one was found in BTO. The band positions, measured at 9 K, for different matrices are listed in Table II.

The absorption spectra of mixed $(1-x)$BSO$\cdot x$BGO crystals were measured in the same spectral regions: bands were detected in the 600–850-, 1300–1700-, and 2000–2500-cm^{-1} ranges. It is worthwhile noting that the bands observed separately in BGO and BSO samples, are present together in the mixed samples; this is shown in Fig. 4, where the spectra in the 1900–2500 region of the two end-members BGO and BSO and of two mixed crystals are displayed as examples. The amplitudes of typical BGO and BSO bands may be seen to scale with the Ge and Si fractions, respectively. This observation is quantitatively confirmed in Fig. 5, where the areas under all BGO lines (in the 1990–2120-cm^{-1} range) and those under all BSO lines (in the 2360–2480-cm^{-1} range) show a rough linear dependence on the Ge and Si fraction, respectively. The BGO bands shift to lower wave numbers by increasing the Ge fraction, while the BSO ones shift to higher wave numbers by decreasing the Si fraction. An example of these trends is given by the insets in Fig. 4 for a BGO band (on the left) and for a BSO band (on the right), respectively. It is noted that the separation between the BGO and BSO lines decreases slightly by increasing the

TABLE II. Band positions at 9 K (in cm^{-1}) for different sillenites are listed considering their attribution. In the BSO column the superscripts α, β, and γ indicate the band positions related to different isotopes, ^{28}Si, ^{29}Si, and ^{30}Si, respectively. The bands attributed to the F-TO and F-LO modes are indicated by the subscripts TO and LO, respectively. The error in the position determination is less than 0.5 cm^{-1}, unless otherwise stated.

	BSO	BGO	BTO
F_{TO}	830.6^{α} $823\pm1^{\beta}$ 817.8^{γ}	679.8	667
F_{LO}	839 ± 1	688 ± 1	680 ± 1
A	785[a]	715[a]	715[b]
$F_{TO}+A$	1607.4^{α} 1602.2^{β} 1595.9^{γ}	1390.7 ± 1	1379.1 ± 1
$F_{LO}+A$	1618.4	1400.7 ± 1	1393 ± 1
$2F_{TO}$	1652.9^{α} 1642.1^{β} 1630.6^{γ}	1355	1336
$F_{TO}+F_{LO}$	1662.3		1348 ± 1
$2F_{LO}$	1674.7 ± 1	1373 ± 1	
$F_{TO}+2A$	2383.4	2100.9	2087 ± 2
$2F_{TO}+A$	2426.8	2064.9	2039.8
$3F_{TO}$	2461.4	2021.7	1987 ± 1
$F_{TO}+3A$	3155.8	2807 ± 2	
$2F_{TO}+2A$	3195.7	2773 ± 2	
$3F_{TO}+A$	3228.1	2731.9	
$4F_{TO}$	3265.1	2687	2645 ± 2

[a]From Ref. 10.
[b]From Ref. 11.

deviation from the extreme compositions (Fig. 4 and Ref. 17).

The temperature dependence of the lines was studied in the 9–300-K range. By increasing the temperature from 9 to 300 K, the bands shift and broaden, and most of the weaker lines and the fine structure are lost: for example, of the ten lines displayed at 9 K in BSO [Fig. 3(b), curve 1] only three are detected at 300 K. The amount and sign of the thermally induced band shift depend both on the specific line and on the M^{4+} considered, as shown in Fig. 6 for the lines displayed in the 1300–2500-cm^{-1} range for a mixed $(1-x)$BSO$\cdot x$BGO sample ($x=0.477$). In this way the behavior of the absorptions typical of BSO and BGO could be contemporaneously investigated in the same sample. With regard to the BGO absorptions, a small "red" shift (i.e., toward the lower wave numbers) is observed for the 1358-cm^{-1} line and a "blue" one for the 1392.7-cm^{-1} line, the shift being less than 2 cm^{-1} over the 9–300-K range [Fig. 6(a)]. Both the BSO lines at 1605.4 and 1652.5 cm^{-1} show blue shifts of 5 and 3.5 cm^{-1}, respectively [Fig. 6(b)]. In the 2000–2400-cm^{-1} range all lines exhibit a blue shift, which is small (2–3 cm^{-1}) for the BGO lines [Fig. 6(c)] and larger (7–13 cm^{-1}) for the BSO lines [Fig. 6(d)]. Small blue shifts are observed for the BSO lines in the region 600–850 cm^{-1}.

IV. DISCUSSION

A. Vibrational modes of the tetrahedral XY_4 molecules and attribution of the observed spectra

The normal vibrations of a free tetrahedral XY_4 molecule are four: ω_1, which is non-degenerate (A-type according to the group theory classification); ω_2, which is doubly degenerate (E type); and ω_3 and ω_4, which are both triply degenerate (F type). Only the F-type vibrations (ω_3 and ω_4) are active in the infrared, while all are Raman active. As a rule, for XY_4 molecules the two highest frequencies are ω_1 and ω_3, the other two being much lower.[20]

As discussed in Sec. I, as a first approximation such a picture can be extended to the vibrations of the tetrahedral MO_4 units in sillenites, although they might be affected slightly by the surrounding network of Bi and O ions. Between the two IR-active frequencies, i.e., ω_3 and ω_4, only the former, being higher, can be separated from the Bi-O vibration modes responsible for the absorption at low wave numbers (below 600 cm^{-1}) and common to all sillenites. Moreover, ω_3 depends on the nature of M^{4+}. Therefore the band observed in the 600–850-cm^{-1} region in Figs. 1(a), 2(a), and 3(a) is attributed to an asymmetric F stretching mode ω_3 of the MO_4 tetrahedral unit.[6,8] We may call the frequency of such a peak ω_F. The symmetric A stretching mode (ω_1) of MO_4 is not IR active and can be detected only by Raman spectroscopy.[9–13]

The two strong lines monitored at wave numbers which are roughly twice ω_F in the range 1300–1700 cm^{-1} are interpreted as a combination band of the F and A modes, and as an overtone of the F mode, respectively. In fact, for example in BGO, the wave number of the peak monitored at 1390.7 cm^{-1} is very close to the sum (1394.8 cm^{-1}) of the F-mode (679.8 cm^{-1}) and A-mode (715 cm^{-1}) wave numbers, and the wave number of the peak detected at 1355 cm^{-1} is very close to twice the F-mode (679.8 cm^{-1}) wave number, 1359.6 cm^{-1} [Table II and Fig. 1(b)]. This means that the absorbed photon simultaneously excites A and F modes in the former case, while it induces a transition from the ground state ($v_3=0$) to the level with $v_3=2$ in the latter (v_j being the vibrational quantum number related to the ω_j mode). The small wave number difference between the calculated and the measured values, which is of the order of a few parts per thousand, is accounted for by anharmonicity effects in Sec. IV C.

Similarly, the bands in the other two regions are attributed to overtone transitions of the F mode ($\Delta v_3=3,4$) and to combination transitions, in which one (or more) F modes (IR active) plus one (or more) A modes (IR inactive) are simultaneously excited. The detailed attribution scheme is reported in Table II.

Therefore, the spectra displayed in Fig. 1 are due to transitions in which only one vibrational mode is excited [Fig.

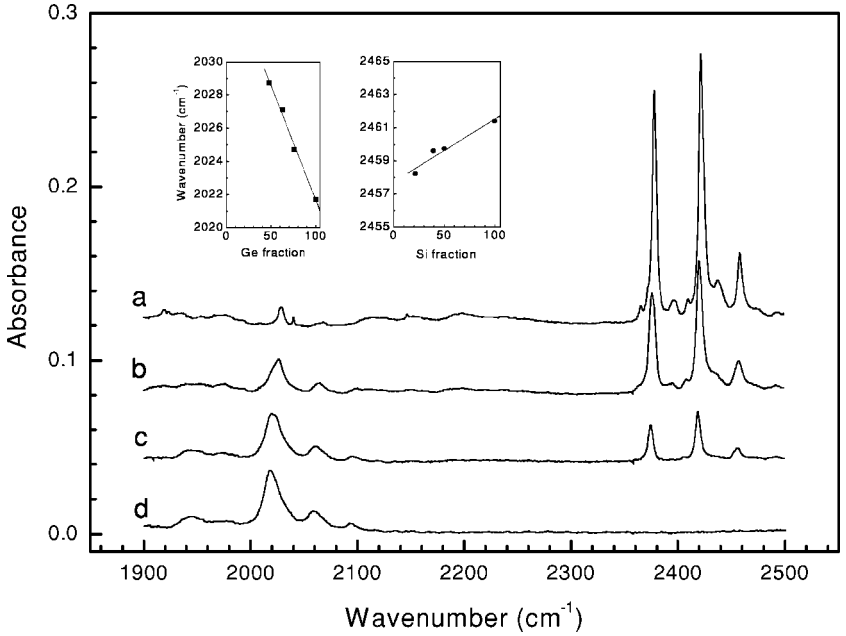

FIG. 4. Spectra in the region 1900–2500 cm^{-1} of $(1-x)$BSO·xBGO crystals: the absorbance is plotted vs the wave number. The thickness of all samples is 1.2 mm. The values of x are the following (according to Table I): curve *a*, $x=0$ (i.e., BSO); curve *b*, $x=0.477$; curve *c*, $x=0.75$; curve *d*, $x=1$ (i.e., BGO). It should be remarked that in the end-member BSO spectrum (curve *a*) the two narrow lines, at ~2045 and 2156 cm^{-1} monitor the presence of S^{6+} traces in the sample, originating from the $F+A$ and $2F$ mode excitations of the SO_4 tetrahedra, respectively (Ref. 21), while the line at ~2030 cm^{-1} is not related to Ge impurities, but rather to a combination of BSO intrinsic vibrational modes. Inserts at the top display the position of the lines due to *F*-mode overtones ($\Delta v_3=3$), as a function of the Ge and Si fractions (listed in Table I) in mixed $(1-x)$BSO·xBGO crystals. The data are taken from curves *a*, *b*, *c*, and *d*, and from the spectrum related to $x=0.63$, not displayed in the figure for the sake of clarity. The left and right panels are related to GeO_4 and SiO_4 vibration modes, respectively. All measurements were performed at 9 K.

1(a)], or two [Fig. 1(b)], or three [Fig. 1(c)], or four [Fig. 1(d)] are simultaneously excited, i.e., one is dealing with the ''multimode'' spectra of BGO. The amplitude of these lines decreases drastically, as expected, by increasing the number of the modes simultaneously excited. This can be verified easily by comparing the thickness of the samples used and the absorbance scale in each of Figs. 1(a), 1(b), 1(c), and 1(d). Similar considerations can be extended to BTO (Fig. 2) and BSO (Fig. 3).

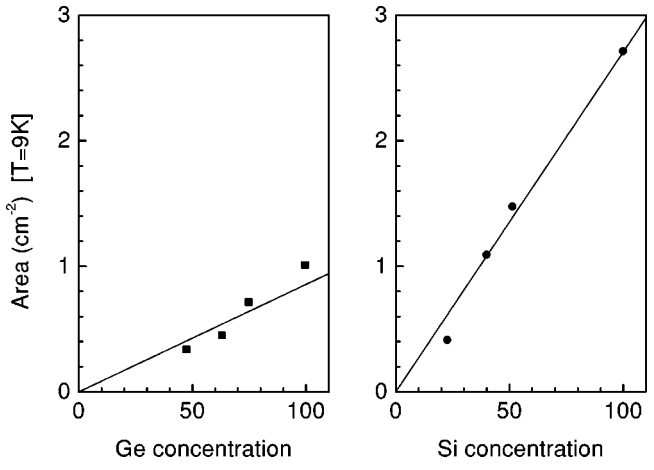

FIG. 5. Area (i.e., absorption coefficient times wave number) under the complex absorption spectrum (Fig. 4) due to the three-mode transitions of the MO_4 tetrahedron vs the M^{4+} fraction (listed in Table I) in mixed $(1-x)$BSO·xBGO crystals. On the left, $M^{4+}=Ge^{4+}$ (the area is evaluated in the 1990–2120-cm^{-1} range); on the right, $M^{4+}=Si^{4+}$ (the area is evaluated in the 2360–2480-cm^{-1} range). The measurements were performed at 9 K.

The basic assumption that the MO_4 vibrations can be regarded as internal vibrations of nearly isolated groups is also supported by comparing, in the $F+A$ and $2F$ mode regions, the absorption spectrum of a pure BSO [Fig. 3(b), curve 1] with that of a BGO, doped with Si (the atomic fraction Si/Ge being ~3.5%), [Fig. 3(b), curve 2]. In this case silicon enters the BGO matrix and substitutes for a germanium tetrahedrally coordinated by four oxygens: thus SiO_4 tetrahedra are ''diluted'' within the BGO matrix.[21,22] Except for a small shift of the peak positions (less than 4 cm^{-1}) toward lower wave numbers in the BGO: Si sample [Fig. 3(b), curve 2] with respect to those in the pure BSO [Fig. 3(b), curve 1], and for the shoulders occurring on the high energy side of the $F+A$ and $2F$ peaks in BSO and missing in BGO: Si, the two spectra are very similar. This similarity stresses that the internal vibrations of the SiO_4 tetrahedra in BSO are practically the same as those of the SiO_4 units diluted into the BGO matrix. Furthermore, the diluted units are affected only weakly by the surrounding GeO_4 tetrahedra. The small peak position shift is accounted for by the larger lattice constant of BGO with respect to that of BSO (Sec. IV D 2), while the absence of shoulders in the BGO: Si spectrum is discussed in detail in Sec. IV B 2.

From an inspection of the data listed in Table II and of Figs. 1–3, where the line attribution is displayed, it turns out

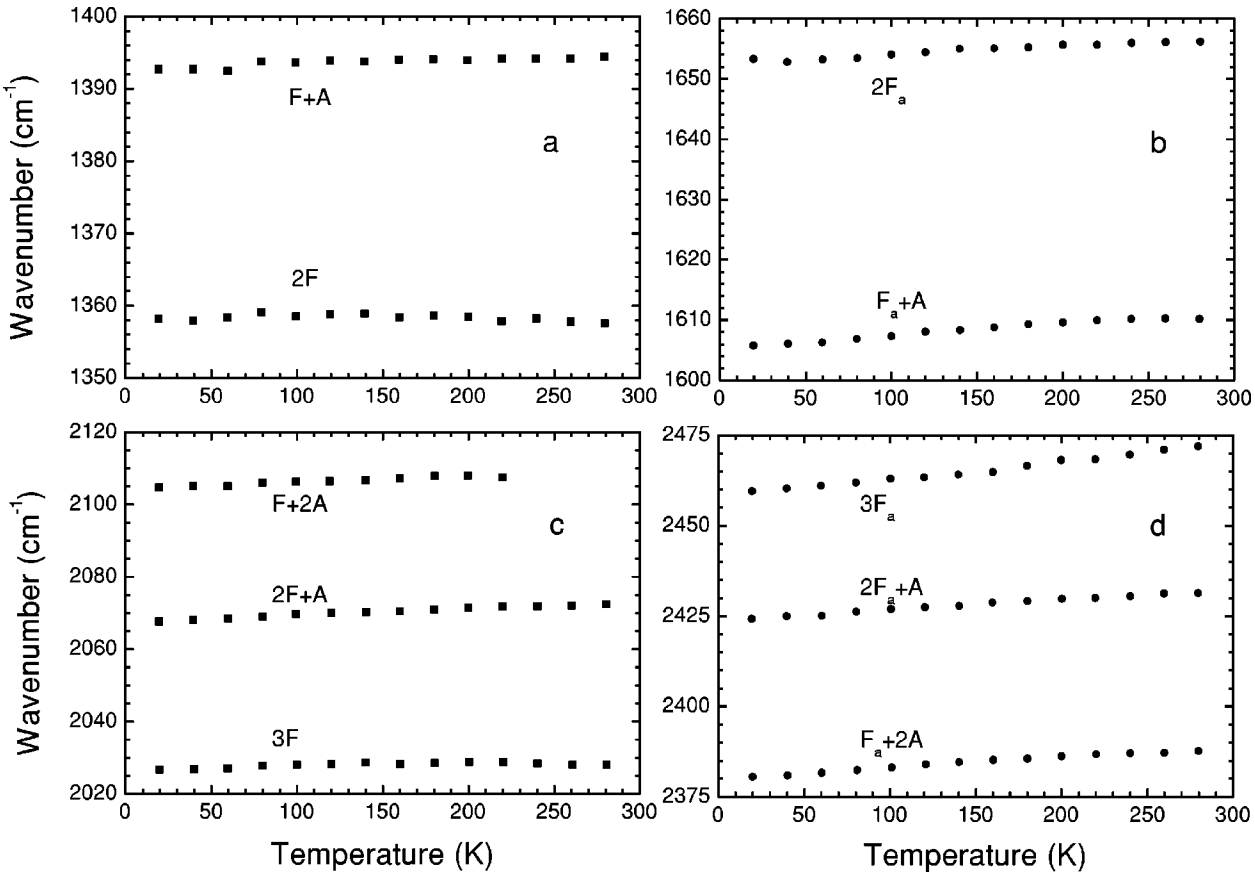

FIG. 6. Temperature dependence of the line positions in the ranges 1300–1700 (two-mode transitions) and 2000–2500 cm^{-1} (three-mode transitions), respectively, in a mixed crystal $(1-x)$BSO$\cdot x$BGO with $x=0.477$.

that in BSO the frequency of the A mode is lower than that of the F mode, while in BGO and BTO the reverse relationship holds. This means that the ratio ω_1/ω_3 depends on the nature of the M^{4+}: such a behavior is consistent with that observed in a wide class of free XY_4 molecules.[20] In fact, both ω_1 and ω_3 depend on the force constant between M^{4+} and O, but the latter depends also on the mass of the central M^{4+} while the former does not, as M^{4+} is immobile in the symmetric mode vibration.[23]

B. Fine structure

It is worthwhile noticing that the spectra of BSO in all regions investigated display a fine structure, which is absent (or, at least is less marked) in BGO and BTO; this is evident, for example, by comparing the two-mode spectrum of Fig. 3(b) (curve 1) with those of Figs. 1(b) and 2(b). This structure can be explained by considering the isotopic effects of M^{4+} and the longitudinal-optical (LO) and transverse-optical (TO) splitting of the F-type ω_3 mode.

1. Isotopic effects

The isotopic effects are particularly evident in the case of BSO. In fact, in addition to the most abundant ^{28}Si (92.21%), ^{29}Si and ^{30}Si are present in natural abundances of 4.7% and 3.09%, respectively. For the one-mode transition two shoulders at wave numbers shorter than ω_F are present.[17] These can be attributed to the isotopic replicas due to ^{29}Si and ^{30}Si of the main peak at 830 cm^{-1} which is due to the most abundant ^{28}Si, in agreement with the Raman spectroscopy results.[9] In the case of the two-mode transitions the isotopic effects are also clearly detectable: it is possible to distinguish the isotopic replicas of the F-mode overtone and of the $F+A$ combination band, as shown by Fig. 3(b) (curve 1). Such peaks are also present in the case of SiO_4 tetrahedra diluted into BGO, as shown in Fig. 3(b) (curve 2).

The above hypothesis can be checked by calculating directly the ω_3 frequency of the SiO_4 unit for the different silicon isotopes. We have done this using the vibrational matrix of Wadia and Balloomal[24] along with the force constants of Wojdowski.[5] For the fundamental F transition the predicted values for the various silicon isotopes are $\omega^{(28)}_{F,calc}=830.0$ cm^{-1}, $\omega^{(29)}_{F,calc}=823.4$ cm^{-1}, and $\omega^{(30)}_{F,calc}=817.0$ cm^{-1}, which may be compared to the measured values, $\omega^{(28)}_{F,expt}=830.6$ cm^{-1}, $\omega^{(29)}_{F,expt}=823\pm1$ cm^{-1}, and $\omega^{(30)}_{F,expt}=817.8$ cm^{-1}. The agreement between the calculated and experimental values is excellent, supporting the above attribution.

The relative amplitude of the peaks can be compared with the natural abundance of the silicon isotopes. This has been done for the $2F$ overtone spectra (which are better resolved than those related to the fundamental F transition), by using different samples. One was a very thin (0.1 mm) BSO crys-

tal: in this way the amplitude of the peak at 1652.9 cm^{-1}, attributed to the most abundant ^{28}Si, could be measured [in the case of a thicker crystal, as that of Fig. 3(b), curve 1, it was out of scale]. The others were two BGO: Si samples, the spectrum of one being displayed by Fig. 3(b) (curve 2): in this way the amplitude of all peaks could be easily measured since the SiO_4 tetrahedra are diluted into the BGO matrix.

The relative amplitudes of the peaks related to ^{28}Si, ^{29}Si, and ^{30}Si were $(92.34 \pm 0.52)\%$, $(4.68 \pm 0.51)\%$, and $(2.98 \pm 0.27)\%$, respectively, while the natural abundances are 92.21%, 4.7%, and 3.09%, respectively. This excellent agreement strongly supports the hypothesis that the isotopic effects are observed in the vibrational spectra of SiO_4 tetrahedra in BSO and BGO sillenites.

BGO and BTO spectra do not show a fine structure, but only a line broadening is observed. In fact, due to the higher atomic masses of Ge and Ti, the relative mass changes, induced by the neighboring isotopes, are small and give rise only to a line broadening.

2. LO-TO splitting of the F mode

Figure 3(b) (curve 1) shows that structures due to isotopic effects in the BSO spectrum appear on the low wavenumber side of the $F+A$ and of the 2F bands, respectively: additional peaks (or shoulders) overlap the high wave number side of the two bands (at 1618.4, 1662.3, and 1674.7 cm^{-1}). Shoulders can be observed on the high wavenumber side of fundamental, overtone, and combination bands of BGO and BTO as well, as noted in Figs. 1(a), 1(b), 2(a), and 2(b), even though they are not as marked as in BSO. Table II summarizes the positions of the additional peaks (or shoulders) for all the sillenites investigated. A possible attribution of the additional peaks to the presence of unwanted impurities can be ruled out since the peaks appear, with the same relative weight, in the spectra of samples grown in different laboratories.

In fact, the shoulders are clearly detectable, for example, in the two-mode spectra of pure BSO samples on the high wave number side of the $F+A$ and $2F$ bands [Fig. 3(b), curve 1], but they either weaken or vanish when the SiO_4 tetrahedra involve Si impurities embedded in a BGO sample [Fig. 3(b), curve 2]. Both spectra show isotopic replicas, indicated by the arrows, while the shoulders are absent in the latter. Similar results are obtained if the SiO_4 tetrahedra are diluted into BTO.[22] Furthermore, the weight of the shoulders is reduced in the two-mode spectra of BSO samples doped with impurities, e.g., Ge^{4+} and P^{5+}.[21,22] The same effect is observed in mixed BSO-BGO samples: one may compare, for example in Fig. 4, the three-mode spectra of the SiO_4 tetrahedra in the region 2300–2500 cm^{-1} of a pure BSO (curve *a*) with that of a mixed $0.25BSO \cdot 0.75BGO$ (curve *c*). According to such results, the shoulders either weaken or disappear if the probability that two or more SiO_4 tetrahedra belong to the same bcc unit cell decreases, as in the case of SiO_4 tetrahedra diluted into a BGO matrix [Fig. 3(b), curve 2], in BSO samples doped with impurities, and in mixed BSO-BGO crystals. In all cases the long-range order of the SiO_4 tetrahedra, typical of the pure BSO matrix, is reduced.

These results are consistent with the attribution of the additional peaks to small longitudinal optical-transverse optical splitting of the *F* mode in the perfect crystal. A similar splitting has been observed in the Raman spectra of BSO and BGO,[10,12,13] and has been derived from the reflectance spectra in BSO, BGO and BTO.[6,7] According to Ref. 10 long-range polarization fields are expected to split the *F* modes into LO-TO modes, with the former at high frequency. The Raman peaks related to these modes were detected at about 828 and 841 cm^{-1} in BSO,[10,12] at 678.6 and 691.8 cm^{-1} in BGO,[10] and at 664 and 687 cm^{-1} in BTO.[13] Mihailova *et al.* carried out calculations which led them to attribute the 828- and 841-cm^{-1} Raman peaks in BSO to the TO and LO *F*-type modes.[12] The reflectance spectra were analyzed by applying the Kramers-Kronig approach[6] and in terms of classical oscillators[7] in order to determine the *F*-TO and *F*-LO mode frequencies. The latter approach, which, according to Ref. 7 provides more reliable values of the optical constants, supplies the following figures for *F*-TO and *F*-LO frequencies: in BSO 833 and 846 cm^{-1}, in BGO 675 and 689 cm^{-1}, and in BTO 660 and 681 cm^{-1}, respectively. The calculated splittings and those derived from the Raman and reflectance measurements, i.e., about 13 and 14 cm^{-1} in BSO and BGO, respectively, are consistent with those noted in Table II, which range from 8.4 to 11 cm^{-1} for BSO and from 8.2 to 10 cm^{-1} for BGO (with some uncertainty in the shoulder peak position). In the case of BTO the discrepancy between the splitting obtained from Raman (23 cm^{-1}) (Ref. 13) and reflectance (21 cm^{-1}) (Ref. 7) measurements and those noted in Table II, which range from 12 to 14 cm^{-1}, is a little larger. However the same trend is observed, i.e., the splitting in BTO is larger than in BSO and BGO. The decrease (or absence) of the shoulders (see above) in the absorption spectra of samples where the long range order of the MO_4 tetrahedra, typical of the pure B*MO* matrix, is reduced provides a further support for the above attribution, in agreement also with Refs. 10 and 13.

As a final comment it should be remarked that, while ordinarily one does not observe LO phonons in IR absorption, in the one-phonon data we deal with small, irregularly shaped particles in a matrix (the KBr pellet; see Sec. II), oriented randomly with respect to the incident beam. It is not implausible that in this case the LO-TO distinction breaks down somewhat. By following the above criteria most of the lines have been assigned to overtones, combination modes, isotopic effects, and LO-TO splitting of the *F* mode, as summarized in Table II and in Figs. 1, 2, and 3.

C. Anharmonicity

The observed peaks have been explained as due to overtones of the *F* mode and to combinations of the *F* and *A* modes. This indicates that the vibrational modes cannot be described as purely harmonic oscillators, for which the transitions $\Delta v_3 \neq 1$ are forbidden, but in addition anharmonicity effects should be considered.

1. F modes

The presence of *F*-mode (ω_3) overtones up to $\Delta v_3 = 4$ shows that anharmonicity affects the asymmetric stretching

of the MO_4 tetrahedron. Therefore, as a first approach, we fitted the observed transition wave numbers (for $\Delta v_3 = 1,2,3,4$) in BSO, BGO, and BTO to those, $G_0(v_3)$, predicted in the framework of the Morse anharmonic oscillator model.[20,25] This model has been successfully applied to diatomic molecules, as for example OH^- in alkali halides,[25–27] in fluoroperovskites,[28] in sillenites,[19] and in other oxides.[29] In the ω_3 mode vibration of the MO_4 group, the displacement of the four oxygens at the corners of the tetrahedron and that of the M^{4+} at the center are along the same direction and opposite from each other.[20] Therefore the vibration can be regarded as that of a diatomic molecule built by the M^{4+} and by a particle with a mass equivalent to that of the four oxygens and located at their center of mass.

The Morse potential is a function of the distance r between the two masses

$$U(r-r_e)=D_{e,3}\{1-\exp[-\beta_3(r-r_e)]\}^2, \qquad (1)$$

where $D_{e,3}$ and β_3 are the potential parameters ($D_{e,3}$ is the binding energy) and r_e is the equilibrium distance. Then for the transition $0\rightarrow v_3$ one obtains

$$G_0(v_3)/v_3=\omega_{e,3}+x_{33}(v_3+1) \qquad (2)$$

where $\omega_{e,3}$ and x_{33} are the zero-order frequency and the anharmonicity constant, respectively, which are functions of the potential parameters.[20] According to Eq. (2) a plot of $G_0(v_3)/v_3$ vs v_3 should give a straight line, from the slope of which one can evaluate x_{33}. This relationship was indeed fulfilled for all the F modes detected (up to $v_3=4$) in BSO, BGO, and BTO as shown in Fig. 7: the x_{33} values are listed in Table III. In addition to the data related to SiO_4, GeO_4, and TiO_4 tetrahedra in BSO, BGO, and BTO, respectively, displayed by squares, Fig. 7 shows the data (triangles) related to the SiO_4 and GeO_4 tetrahedra diluted in BGO (top) and BSO (middle), respectively. The result provides further support to the assumption that the internal vibrations of the MO_4 tetrahedra in $Bi_{12}MO_{20}$ are practically the same as those of an isolated MO_4 tetrahedron diluted into a sillenite matrix in which the host tetravalent ion is different from M.

Thus the asymmetric F stretching mode of the tetrahedron can be satisfactorily described by the Morse model, which was proposed originally for a simple free diatomic molecule. This confirms the hypothesis according to which the measured frequencies ω_F in BGO and BSO ($\Delta v_3=1$) fit quite well the highest of the normal-mode frequencies of GeO_4 and SiO_4 molecular groups.[5]

The anharmonicity parameters for the tetrahedral vibration of the MO_4 unit $x_e\equiv|x_{33}/\omega_{e,3}|$ are 0.006, 0.004, and 0.003 for BSO, BGO, and BTO, respectively. These are smaller than that ($x_e\sim 2.5\times 10^{-2}$) reported for the localized mode induced by OH in the same matrices.[19] However, at least in the case of BSO, the value of D_e is nearly the same for both molecular groups, i.e., 4.69 and 4.42 eV for MO_4 and OH,[19] respectively. The difference in anharmonicity parameters arises from the difference in reduced masses μ. The anharmonicity parameter is proportional to $\mu^{-1/2}$; therefore,

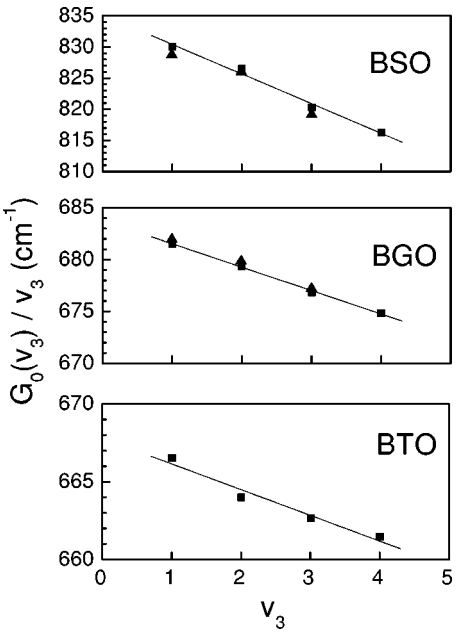

FIG. 7. Anharmonicity of the F modes in BSO, BGO, and BTO crystals: the ratio between the measured wave number $G_0(v_3)$ of the $0\rightarrow v_3$ transition and the vibrational quantum number v_3 is plotted vs v_3. The squares give the experimental data and the solid line is the fitting according to Eq. (2). For BSO the squares are related to the lines due to ^{28}Si. The triangles are related to $^{28}SiO_4$ tetrahedra "diluted" into BGO (top) and to GeO_4 tetrahedra "diluted" into BSO (middle).

since the reduced mass of the OH oscillator is 5% of that of the MO_4 unit, the anharmonicity parameter of the OH is about 4.5 times as large as that of SiO_4. Furthermore, the amplitude of the oscillations of OH is larger, even in the ground state. This effect is even more pronounced in the excited states, since the zero-order vibration frequency of OH is higher ($\omega_e=839.9$ and 3626.46 cm^{-1} for MO_4 and OH, respectively). This means that OH, when oscillating, experiences regions in which the potential shape deviates meaningfully from the harmonic one, while the heavier MO_4 molecule oscillates nearer the bottom of the potential well, where the harmonic approximation still holds rather well.

The anharmonicity parameter of the MO_4 group, as for OH^- in sillenites,[19] decreases by increasing the lattice constant. This behavior is opposite to that observed for OH^- in a large variety of alkali halides, where the anharmonicity parameter increases by increasing the lattice constant.[27] The discrepancy can be explained by considering that in a simple lattice, as that of alkali halides, the lattice constant is closely related to the distance between the oscillator (OH^-) and the nearest neighbors (the alkali ions). Such a relationship does not hold for a more complex structure, as that of the sillenites with 66 atoms per cubic unit cell.[4] In fact, the distance between the oxygens, sitting at the corners of the MO_4 tetrahedron, and the neighboring Bi decreases by increasing the lattice constant.[30] Therefore, the behavior of the anharmonicity parameter vs the nearest neighbor distance for MO_4 and OH in sillenites shows the same trend displayed by OH^- in alkali halides.

TABLE III. Morse parameters, i.e., zero-order frequencies $\omega_{e,1}$ and $\omega_{e,3}$, anharmonicity constants x_{11}, x_{13}, and x_{33}, and binding energy $D_{e,3}$ calculated using Eqs. (2) and (3) for BSO, BGO, and BTO.

Matrix	$\omega_{e,1}$ (cm^{-1})	$x_{1,1}$ (cm^{-1})	$x_{1,3}$ (cm^{-1})	$x_{3,3}$ (cm^{-1})	$\omega_{e,3}$ (cm^{-1})	$D_{e,3}$ (eV)
BSO				-4.9 ± 0.2[a]	835.7 ± 0.7[a]	4.69 ± 0.06
	788.6 ± 5.2[b]	-1.5 ± 0.8[b]	-5.1 ± 1.4[b]	-4.8 ± 0.6[b]	842.0 ± 4.1[b]	
BGO				-2.9 ± 0.2[a]	682.8 ± 0.6[a]	5.46 ± 0.14
	713.5 ± 2.5[b]	-1.1 ± 0.5[b]	-0.3 ± 0.7[b]	-2.2 ± 0.3[b]	681.7 ± 2.0[b]	
BTO				-1.9 ± 0.4[a]	668.4 ± 0.8[a]	8.6 ± 0.4
	717.7 ± 0.2[b]	-1.9 ± 0.4[b]	-0.7 ± 0.6[b]	-1.1 ± 0.2[b]	666.7 ± 1.3[b]	

[a]From the experimental data fitting to Eq. (2).
[b]From the experimental data fitting to Eq. (3).

2. General approach

A more general description of the anharmonicity, affecting the MO_4 tetrahedron vibrations, can be obtained by considering also the *A*-symmetric mode in addition to the *F*-asymmetric ones. By following the approach suggested by Herzberg[20] for a polyatomic anharmonic molecule with *m* normal vibrations, characterized by the zero-order frequencies $\omega_{e,j}$ (with $j=1,2,\ldots,m$), the frequency $G_0(v_1,v_2,\ldots)$ for the transition $0,0,\ldots\rightarrow v_1,v_2,\ldots$ is given by

$$G_0(v_1,v_2,\ldots)=\sum_{j=1}^{m}\omega_j^0 v_j+\sum_j\sum_{k\geq j}x_{jk}v_jv_k+\cdots, \quad (3)$$

where

$$\omega_j^0=\omega_{e,j}+x_{jj}+\frac{1}{2}\sum_{k\neq j}x_{jk}+\cdots, \quad (4)$$

v_j is the vibrational quantum number corresponding to each normal vibration, and x_{jk} is the anharmonicity constant. The terms of order higher than the second in the vibrational quantum numbers and higher than the first in the anharmonicity constants are neglected.

Such a description can be applied to the present absorption spectra due to the *F*-mode fundamental and overtone transitions (ω_3), to combination transitions, in which *F* (ω_3) and *A* modes (ω_1) are simultaneously excited, and to the Raman-active *A* mode,[9–13] (Table II). By substituting in Eq. (3) the experimental values of $G_0(v_1,0,v_3,0)$ (with $v_1=0,1,2,3$ and $v_3=0,1,2,3,4$) listed in Table II, one obtains a set of equations (11 for BSO and BGO and eight for BTO) from which one obtains the values of $\omega_{e,1}$, $\omega_{e,3}$, x_{11}, x_{13}, and x_{33}. The results are collected in Table III. It is noted that $\omega_{e,j}$ ($j=1,3$), evaluated in this way, contains an additional term $\frac{1}{2}\Sigma x_{jk}$ ($k=2,4$). In fact, such a term does not behave as an independent variable in the above set of equations, since data about transitions, in which $\omega_{e,2}$ and/or $\omega_{e,4}$ modes are excited, are not available. The agreement between the values of $\omega_{e,3}$ and of x_{33} obtained by using the fitting of the experimental data to Eq. (2) and those calculated from Eq. (3) is rather good, confirming the weak anharmonicity effects associated with the ω_3 mode. The error which affects the anharmonicity x_{11} of the A symmetric stretching mode (ω_1) and the mixed x_{13} is rather large; however it turns out they are still lower than the anharmonicity of the *F* mode (except for the case of BTO).

D. Mixed crystals

A similar analysis has been extended to the mixed $(1-x)$BSO·xBGO crystals. The overtone spectra (detected up to $v_3=3$) typical of BGO and BSO were both present, as well as the combination of *A* and *F* modes, as shown in Fig. 4.

1. Two-mode behavior

In terms of their spectral behavior, mixed crystals may be classified into different classes[18] as follows.

(i) One-mode behavior: this is typified by a single optically active mode whose frequency varies continuously from the frequency characteristic of one end member to that of the other end-member with the mode strength remaining approximately constant.

(ii) Two-mode behavior: two optical mode frequencies in the mixed crystal are observed to occur close to the end-member frequencies. The relative strength and the frequency of each mode are approximately proportional to the fraction of the formula weight of each component.

(iii) Mixed one mode-two mode behavior.

$(1-x)$BSO·xBGO mixed crystals show a typical two-mode behavior. In fact, both BGO and BSO characteristic bands are present in the two- and three-mode absorption spectra of the mixed crystals (Fig. 4). The shift of each line with respect to the position observed in the end-member crystals (i.e., $x=0$ or $x=1$) was found to be a linear function of x or $(1-x)$, respectively, as shown in the inserts of Fig. 4 for the two overtones $\Delta v_3=3$ of GeO_4 and SiO_4 vibrations, respectively. Such a linearity is observed only if the x values are those obtained from the chemical analysis of Si and Ge performed on the samples investigated, and not the nominal ones (i.e., in the melt) (Table I). The relative strength of the GeO_4 and SiO_4 modes, as monitored by the area under the related absorption spectra, is approximately proportional to the Ge and Si concentration (Fig. 5), matching in this way the last requirement for a two-mode behavior.

It should be emphasized that the BSO lines in the mixed crystals are slightly broader and show a less sharp fine struc-

ture (see Sec. IV B) than the corresponding ones in the end-member BSO (compare, for example, curves *a* and *b* in Fig. 4). Such a result can be understood considering a random distribution of Ge^{4+} and Si^{4+} ions at the M^{4+} positions at the center of the tetrahedra; therefore the Si isotopes experience slightly different surroundings which cause a line broadening and overlapping. Similar line broadening effects were detected for the OH^- absorption in the mixed sillenites.[19]

As a concluding remark, the two-mode behavior[18] well describes the MO_4 tetrahedron stretching modes in $(1-x)\mathrm{BSO}\cdot x\mathrm{BGO}$ mixed crystals, not only for the fundamental transitions, as previously reported,[31,32] but also for the overtones and the combination transitions (at least up to three-mode transitions) as supported by the position and the amplitude of the lines.

2. Vibrational mode-Grüneisen constants

By changing the value of *x* the lattice constant *a* changes as well, from the value typical of BGO ($a=10.13281$ Å) to that of BSO ($a=10.09404$ Å) (Ref. 19): this means that in mixed crystals the vibrations (*F* and *A* modes) of the GeO_4 tetrahedron take place in a compressed lattice (in comparison to that of the BGO end member), while those of SiO_4 occur in an expanded lattice (in comparison to that of the BSO end member). Since the harmonic force constant of the oscillator may be a function of the volume (i.e., of the lattice constant), there is a lattice constant dependence of the vibrational frequencies,[31] in addition to the anharmonic effects which are manifested through the temperature change as noted in Sec. IV E. As a rule, the vibrational frequencies decrease as a consequence of the lattice expansion.[31] Therefore in the mixed crystals the SiO_4 tetrahedron vibrational frequencies should decrease, since the vibration occurs in an expanded lattice, while those of the GeO_4 group should increase since the vibration occurs in a compressed lattice. This conclusion is supported by present experimental results (Fig. 4 and Ref. 17). Moreover, since the lattice constants of the mixed crystals investigated are known,[19] the vibrational mode-Grüneisen constant γ_{ω_j} can be evaluated from the frequency dependence on the lattice constant (i.e., volume).[31] In fact, one has

$$\gamma_{\omega_j}=-\frac{1}{3}\times\frac{d\log(\omega_j/\omega_{j,0})}{d\log(a/a_0)}, \tag{5}$$

where $\omega_{j,0}$ and a_0 are the frequency and the lattice constant of the unperturbed lattice (or of the end-member system, i.e., $x=0,1$) and ω_j and *a* are the same parameters for the perturbed (compressed or expanded) lattice (or for the mixed crystals, i.e., $0<x<1$). For the mixed crystals the range of the (a/a_0) values, and consequently of the $(\omega_j/\omega_{j,0})$, is very small (a few thousandths), therefore only a hint on the values of vibrational mode-γ's at 9 K can be obtained. They are the following: $\gamma_{2F+A}\sim\gamma_{F+2A}\sim\gamma_{3F}\sim 0.2$ for SiO_4 vibrations, and $\gamma_{2F+A}\sim 0.4, \gamma_{3F}\sim 0.6$ for GeO_4 vibrations. The present figures are lower than those $(1<\gamma<3)$ evaluated from compressibility *K*, thermal expansion coefficient α_V, specific heat C_V, and volume *V*, according to

$$\gamma=\alpha_V V/KC_V \tag{6}$$

for a wide class of materials (for example metals and alkali halides) at room temperature. The discrepancy can be accounted for by considering that the present γ_{ω_j}'s are related to single well defined vibration modes, and are not averaged on all lattice modes as in the case of γ calculated from macroscopic parameters, according to Eq. (6). Moreover they are evaluated at low temperature (9 K), where the vibrational mode Grüneisen ''constant'' is expected to decrease considerably[33,34] with respect to the high temperature value. The fact that the γ related to the GeO_4 vibrations is higher than that related to the SiO_4 vibrations is consistent with the higher microhardness (inversely proportional to the compressibility *K*) exhibited by BGO in comparison with that of BSO, while the thermal expansion and specific heat values are very similar for the two systems.[1]

E. Temperature dependence

The temperature induced shift of a given mode frequency and, as a consequence, of the line position is due to the anharmonic coupling of the mode in question with phonons and to the thermal expansion of the crystal. Although the thermal expansion itself occurs as a result of anharmonicity, it affects the ''quasiharmonic'' frequencies through the harmonic force constant, which may change with the volume. Often the direction of the shift arising from the two effects (thermal expansion and anharmonicity) may be opposite. As a rule the thermal expansion induces a ''red'' shift of the lines. The anharmonicity effect is split into two contributions: the former arises from the coefficient K_3 of the cubic term (in the expression of the anharmonic potential as a function of the ion separation), while the latter arises from the coefficient K_4 of the quartic term. While the former gives rise to a shift of the same sign as that induced by the thermal expansion (i.e., a red shift), the latter works in the opposite direction (i.e., a blue shift).[31,35] For the transverse optical modes of LiF and MgO a red shift has been observed as a function of the temperature, even though the shift amount was smaller than that expected as a result of the thermal expansion.[31] This smaller shift could be explained by considering the opposite contribution arising from the anharmonicity. In the case of the tetrahedral unit vibrations in sillenites the lines attributed to the *F* overtones and to the combination modes (F,A) exhibit a prevailing blue shift as the temperature increases (Sec. III and Fig. 6). This result can be accounted for by assuming that the anharmonicity contribution to the shift given by the K_4 coefficient prevails over those induced by the thermal expansion and K_3. It should be remarked that the thermal expansion coefficients of BSO and BGO are of the order of 16×10^{-6} K^{-1} (for $T>300$ K),[1] considerably lower than that of LiF ($>100\times10^{-6}$ K^{-1}) in the same temperature range.[36] Moreover the anharmonic effects could play a more important role in the present case, compared to LiF and MgO, since the *F* mode (fundamental and overtones) and the combination (F,A) transitions occur at higher energies; therefore, the oscillating atoms experience a more anharmonic region of the potential well. According to

Zhang a blue shift may occur when the K_4 coefficient is positive.[35] Such a preliminary requirement is fulfilled by the Morse potential which, according to Sec. IV C, describes quite satisfactorily the interaction between M^{4+} and the four oxygen ions in sillenites.

As a final comment, it should be remarked that the slight disorder present in the mixed samples causes an inhomogeneous broadening of the lines, as expected, but does not affect the temperature dependence of the line positions. In fact, for example, the trends of the $2F$ and $F+A$ mode position vs temperature in pure BSO were the same as those displayed in Fig. 6 and related to the mixed crystal ($x=0.477$), the unique difference being a small shift to higher wave numbers, as expected, on the basis of a smaller lattice constant.

V. CONCLUSIONS

Most of the structures shown at 9 K by the infrared spectra of sillenites in the 600–3500-cm^{-1} range can be understood by considering the asymmetric F and symmetric A modes of the MO_4 (M=Ge,Si,Ti) tetrahedral vibrations. Absorptions are due to (1) combination modes, i.e., one or more F modes (IR active) + one or more A modes (IR inactive) are simultaneously excited; (2) overtone transitions of the F mode; (3) isotopic effects, which are particularly relevant in the case of BSO, since in addition to the most abundant ^{28}Si (92.2%) there are also ^{29}Si and ^{30}Si present in natural abundances of 4.7% and 3.1% respectively; and (4) LO-TO splitting of the F modes.

The anharmonicity of the F and A modes was calculated for BSO, BGO, and BTO by using simple models for the anharmonic oscillator. The tetrahedral vibrations in $(1-x)$BSO$\cdot x$BGO mixed crystals show a characteristic two-mode behavior up to three-mode transitions. In fact, both BGO and BSO characteristic absorptions are present, the frequencies are linearly dependent on the composition, and the relative strengths are approximately proportional to the Ge and Si concentrations, respectively.

The temperature dependence of the band position was also studied, mainly in the mixed crystals: the blue shift observed over the 9–300-K range for many lines is interpreted by assuming a dominant role played by the anharmonicity contribution described by the K_4 coefficient as compared with that coming from the thermal expansion

ACKNOWLEDGMENTS

The authors wish to thank Dr. O. Szakács of the Research Institute for Solid State Physics and Optics, Hungarian Academy of Sciences, Budapest for the chemical analysis of the samples, and Dr. M. Gospodinov of the Institute of Solid State Physics, Bulgarian Academy of Sciences, Sofia, for supplying a few sillenite samples doped with impurities. One of the authors (L.K.) undertook this work with the support of the ICTP Program for Training and Research in Italian Laboratories, Trieste, Italy. Financial support from the National Fund of Hungary (OTKA No. T22859) and from the Italian Institute for Physics of Matter (INFM) is also acknowledged. Part of the research was carried out in the framework of the Agreement for Scientific and Technological Cooperation between the National Research Council of Italy and the Hungarian Academy of Sciences. The technical help of Carlo Mora of IMEM-CNR Institute of Parma is also acknowledged.

[1] L. Arizmendi, J. M. Cabrera, and F. Agulló-López, Int. J. Optoelectron. **7**, 149 (1992).
[2] *Photorefractive Materials and Their Applications I and II*, edited by P. Gunter and H. P. Huignard, Topics in Applied Physics Vols. 61 and 62 (Springer, Berlin, 1988).
[3] S. L. Hou and D. S. Oliver, Appl. Phys. Lett. **18**, 325 (1971).
[4] S. C. Abrahams, P. B. Jamieson, and J. L. Bernstein, J. Chem. Phys. **47**, 4034 (1967).
[5] W. Wojdowski, Phys. Status Solidi B **130**, 121 (1985).
[6] W. Wojdowski, T. Łukasiewicz, W. Nazarewicz, and J. Żmija, Phys. Status Solidi B **94**, 649 (1979).
[7] E. Burattini, G. Cappuccio, M. C. Ferrari, M. Grandolfo, P. Vecchia, and Sh. Efendiev, J. Opt. Soc. Am. B **5**, 714 (1988).
[8] W. Wojdowski, Phys. Status Solidi B **123**, K101 (1984).
[9] M. V. Belousov, E. I. Leonov, and A. G. Shcherbakov, Fiz. Tverd. Tela (Leningrad) **28**, 598 (1986) [Sov. Phys. Solid State **28**, 336 (1986)].
[10] S. Venugopalan and A. K. Ramdas, Phys. Rev. B **5**, 4065 (1972).
[11] Yu. G. Zaretskii, G. A. Kurbatov, V. V. Prokofev, Yu. I. Ukhanov, and Yu. V. Shmartsev, Opt. Spektrosk. **54**, 569 (1983) [Opt. Spectrosc. **54**, 338 (1983)].
[12] B. Mihailova, M. Gospodinov, and L. Konstantinov, J. Phys. Chem. Solids **60**, 1821 (1999).
[13] B. Mihailova, G. Bogachev, V. Marinova, and L. Konstantinov, J. Phys. Chem. Solids **60**, 1829 (1999).
[14] M. V. Belousov, E. I. Leonov, V. D. Petrikov, and A. G. Shcherbakov, Fiz. Tverd. Tela (Leningrad) **30**, 396 (1988) [Sov. Phys. Solid State **30**, 226 (1988)].
[15] A. V. Khomich, M. G. Ermakov, P. I. Perov, and V. V. Kucha, Zh. Prikl. Spektrosk. **40**, 387 (1982).
[16] A. V. Khomich, Yu. F. Kargin, P. I. Perov, and V. M. Skorikov, Inorg. Mater. (Transl. of Neorg. Mater.) **26**, 1635 (1990).
[17] P. Beneventi, R. Capelletti, and L. Kovács, Radiat. Eff. Defects Solids **134**, 293 (1995).
[18] L. Genzel, T. P. Martin, and C. H. Perry, Phys. Status Solidi B **62**, 83 (1974).
[19] P. Beneventi, R. Capelletti, L. Kovács, Á. Péter, A. M. Lanfredi Manotti, and F. Ugozzoli, J. Phys.: Condens. Matter **6**, 6329 (1994).
[20] G. Herzberg, *Molecular Spectra and Molecular Structure II. Infrared and Raman Spectra of Polyatomic Molecules* (Van Nostrand Reinhold, New York, 1945).
[21] R. Capelletti, P. Beneventi, L. Kovács, and A. Ruffini, Ber. Bunsenges. Phys. Chem. **101**, 1282 (1997).
[22] E. Bandini, P. Beneventi, D. Bersani, R. Capelletti, M. Gospodi-

nov, and L. Kovács, Mikrochim. Acta, Suppl. **14**, 489 (1997).
[23] M. Devalette, J. Darriet, M. Couzi, C. Mazeau, and P. Hagenmuller, J. Solid State Chem. **43**, 45 (1982).
[24] W. Wadia and L. S. Balloomal, Phys. Chem. Glasses **9**, 115 (1968).
[25] W. B. Fowler, R. Capelletti, and E. Colombi, Phys. Rev. B **44**, 2961 (1991).
[26] R. Capelletti, P. Beneventi, E. Colombi, and W. B. Fowler, Nuovo Cimento D **15**, 415 (1993).
[27] Ch. P. Afanasiev and F. Lüty, in *Defects in Insulating Materials*, edited by O. Kanert and J.-M. Spaeth (World Scientific, Singapore, 1993), Vol. 1, p. 551, and private communication.
[28] A. Baraldi, P. Bertoli, R. Capelletti, A. Ruffini, and A. Scacco, Phys. Rev. B **63**, 134302 (2001).
[29] M. Wöhlecke and L. Kovács, Crit. Rev. Solid State Mater. Sci. **26**, 1 (2001).
[30] Yu. G. Zaretskii, Yu. I. Ukhanov, and Yu. V. Shmartsev, Fiz. Tverd. Tela (Leningrad) **33**, 1210 (1991) [Sov. Phys. Solid State **33**, 685 (1991)].
[31] S. S. Mitra, in *Infrared and Raman Spectra due to Lattice Vibrations (Optical Properties of Solids)*, edited by S. Nudelman and S. S. Mitra (Plenum Press, New York, 1969), p. 333.
[32] D. Senulienè and G. Babonas, Phys. Status Solidi B **180**, 541 (1993).
[33] J. F. Vetelino, K. V. Namjoshi, and S. S. Mitra, J. Appl. Phys. **41**, 5041 (1970).
[34] W. Daniels, J. Phys. Chem. Solids Suppl. **1**, 273 (1965).
[35] Z. Y. Zhang, Phys. Lett. A **143**, 413 (1990).
[36] *American Institute of Physics Handbook*, 2nd ed. (McGraw-Hill, New York, 1957), pp. 4–73.